A New Iterative Diakoptics-Based Multilevel Moments Method for Planar Circuits

Steven Ooms, *Student Member, IEEE*, and Daniël De Zutter, *Senior Member, IEEE*

***Abstract*—This paper combines a multilevel moments method (MMM) scheme with a modified diakoptics (MD) technique and a block Gauss–Seidel (BGS) iterative technique to reduce the solution time of large planar microwave structures. The proposed MMM scheme has two levels. On the lower level, the planar circuit is divided into several subcircuits using two types of artificial ports. At the higher level, general basis functions defined over the complete circuit are generated in an iterative way. The validity and the efficiency of the new technique are validated by several examples, including a large low-pass filter.**

I. Introduction

IN ORDER TO reduce the development cost and shorten the development cycle of electromagnetic high frequency (HF) circuits, developers use computer-aided design (CAD) techniques to predict the performances of the circuit even before it is ever built. Today, circuit simulators are quite popular and have become a standard tool for a developer. For dense and complex structures with strong or important parasitic couplings, the accuracy of these circuit simulators is often limited. In those cases, electromagnetic simulators are of growing importance.

Electromagnetic field (EM) simulations based on the method of moments (MoM) [1] are highly accurate and applicable to HF planar circuit design [2]–[5]. However, the MoM needs a lot of memory and solution time for large circuits, severely limiting its application.

Several techniques have been used to overcome these limitations. For large scatterers, a spatial decomposition technique [6], [7], multilevel methods in combination with the fast multipole method [8], [9], and an MMM [10] have been successfully applied. For wire antenna problems, a diakoptic technique based on network impedances was developed in [11] and improved with an iterative scheme in [12] and [13]. As mentioned in [14], this diakoptic technique can be interpreted as a MoM technique.

A combination of the MMM and the diakoptic technique (as suggested in [14]) was also applied to planar microwave structures in [15] and [16], without any iterative refinement. In [17], a multigrid method similar to the MMM in [10] was interpreted as an iterative diakoptic method. In [18], a two-level spectral technique was proposed in the spectral domain.

However, in this paper we will combine the MMM, a diakoptic technique, and an iterative approach in order to solve the MoM matrix equation resulting from an EM simulation of planar microstrip circuits. We will do this faster and by using less memory than the direct solution, given only the system Z-matrix and a subcircuit division. We start from the MMM technique outlined in Section II. The addition of an iterative refinement is described in Section III. Our technique is then validated by some examples in Section IV, followed by some concluding remarks in Section V.

Manuscript received December 9, 1996; revised September 18, 1997. This work was supported by the Belgian National Funds for Scientific Research (NFWO).

S. Ooms was with the Department of Information Technology (INTEC), University of Gent, B-9000 Gent, Belgium. He is now with BARCO Chromatics, Kortrijk, B-8500 Belgium.

D. De Zutter is with the Department of Information Technology (INTEC), University of Gent, B-9000 Gent, Belgium (e-mail: daniel.dezutter@intec.rug.ac.be).

Publisher Item Identifier S 0018-9480(98)02025-0.

II. Multilevel Moments Method

A. The General Principle

An MMM simulation [10], [15], [16] of an electromagnetic circuit consists of two phases. During the first top–down phase, the circuit is divided into several subcircuits by artificial ports (as opposed to the original exterior ports). Each subcircuit is again divided into sub-subcircuits, and so on until the lowest level is reached. On the lowest level, the current density is discretized using a set of basis functions such as pulse basis functions or rooftop functions, just as in an ordinary MoM simulation [1].

During the second bottom-up phase, a MoM simulation is applied to the lowest level by exciting the (lower level) ports—both exterior and artificial—one after the other. The resulting current densities on each subcircuit form "generalized half rooftop functions" and are combined into "generalized (full) rooftop functions" at the artificial ports by demanding current continuity at these ports. These "generalized (full) rooftop functions" are used as the basis functions for the next level. This process is repeated up to the upper level, each time using the results of the previous level as basis functions for the next one. Due to the variational character of the MoM [11], [19], the errors made by using coarser basis functions instead of the finer ones on the lowest level reduce quadratically on the next level.

B. Two-Level MMM

In our approach, we apply a two-level MMM scheme with rooftop basis functions [3] on the lowest level to planar microwave circuits. We will illustrate our approach using a microstrip transmission line (Fig. 1(a), with two exterior ports P_1 and P_2). First, the circuit is divided into several subcircuits

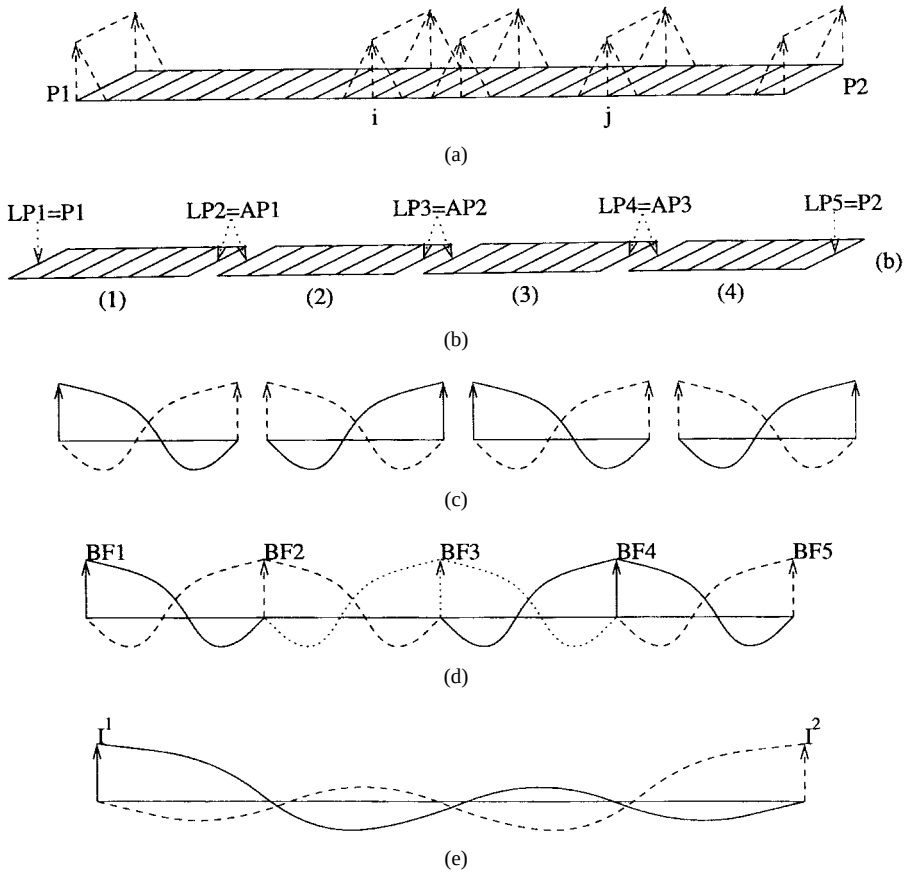

Fig. 1. Two-level moments method.

by inserting artificial ports (in Fig. 1(b), we added three artificial ports—AP_1, AP_2, and AP_3—yielding four subcircuits). Each of these subcircuits is then simulated separately for as many excitations as the considered subcircuit has (lower level) ports: we apply a unit current at the excited port, while leaving the unexcited ports open. The current density profiles resulting from these lower level MoM's are shown in Fig. 1(c) (eight in total). They can be thought of as "generalized half rooftop" functions at the lower level ports. By demanding current continuity at the portsides of the artificial ports, these profiles are combined into "generalized (full) rooftop" functions (in Fig. 1(d), the eight profiles from Fig. 1(c) are combined into five upper level basis functions BF_k). These "generalized rooftop" functions form the basis functions BF_k for the upper level MoM.

During the upper level MoM, we simulate the complete circuit under the excitation of the exterior ports using the "generalized rooftop" functions BF_k as basis functions. In other words, we are interested in finding the amplitudes A_{ke} of these "generalized rooftop" basis functions when exciting the exterior port P_e. The resulting MoM equation is then

$$\forall e \in P, \forall k \in LP: \sum_{l \in \mathrm{LP}} Z_{kl}^{\mathrm{up}} A_{le} = V_{ke}^{\mathrm{up}} \tag{1}$$

with P, AP, and LP $(= P \cup AP)$, respectively, the set of the exterior ports, the artificial ports, and the lower level ports (in the example of Fig. 1: $P = 1, 2$; $AP = 1, 2, 3$; $LP = 1, 2, 3, 4, 5$) and V_{ke}^{up} the excitation term due to the excitation of exterior port P_e. The upper level Z-matrix elements Z_{kl}^{up} describe the coupling between two basis functions BF_k and BF_l. They can be derived directly from the lower level matrix elements Z_{ij}, which describe the coupling between the lowest level rooftop functions on side i and side j:

$$Z_{kl}^{\mathrm{up}} = \sum_{i \in \mathrm{BF}(k)} \sum_{j \in \mathrm{BF}(l)} I_{ik}^{\mathrm{bf}} Z_{ij} I_{jl}^{\mathrm{bf}}. \tag{2}$$

The coefficients I_{ik}^{bf} must be interpreted as follows. The "generalized rooftop" basis functions BF_k—k indicates lower level port LP_k is excited and is also the second subindex of I_{ik}^{bf}—are formed by individual contributions of the lowest level rooftop functions used for the lower level MoM. The resulting amplitude of each such rooftop basis function at side i is precisely I_{ik}^{bf}. Hence, according to (2), Z_{kl}^{up} can be interpreted as the sum of the individual Z_{ij} weighted quadratically by the "generalized rooftop" basis function profiles k and l, all expressed as a function of the lowest level rooftop functions.

The quantities we are finally interested in are the overall current densities I^e [Fig. 1(e)] due to the excitation of exterior port P_e, expressed as a function of the amplitudes I_{ie} of the lowest level rooftop functions over side i. These current densities can be found as the linear combination of the profile of each "generalized rooftop" basis function BF_k multiplied by its amplitude, which was calculated during the upper level MoM. In other words, the overall current density I_{ie} at side i when exciting exterior port P_e can be found as the summation over the product of the amplitude of the current profile of the

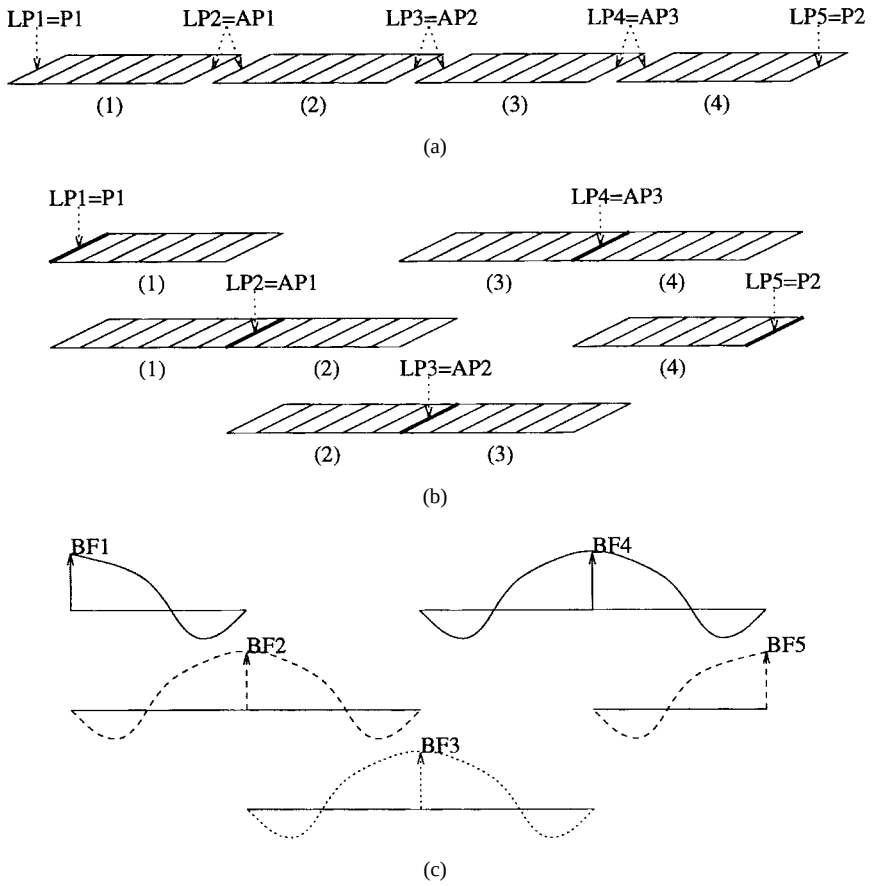

Fig. 2. Two-level moments method: FAP.

"generalized rooftop" basis function BF_k at side i, i.e., I_{ik}^{bf}, with the amplitude of the "generalized rooftop" basis functions BF_k when exciting exterior port P_e, i.e., A_{ke}:

$$\forall e \in \mathrm{P}, \forall i \in S\colon I_{ie} = \sum_{k \in \mathrm{AP}} I_{ik}^{\mathrm{bf}} A_{ke}. \tag{3}$$

These overall current densities I_{ie} are supposed to be a good approximation of those yielded by one direct MoM. It should be noted that coupling between all subcircuits is taken into account, but only as the coupling between the "generalized rooftop" basis functions as a whole, and not as the coupling between the individual lowest level rooftop basis functions as when solving the problem directly.

Also note that in (2), I_{ik}^{bf} is only defined in the subcircuits connected to lower level port LP_k (zero on the other subcircuits) which reduces the number of operations for the double summation.

C. FAP's and SAP's

During the lower level MoM simulation of one subcircuit the presence of the other subcircuits was neglected [Fig. 1(c)]. When constructing the "generalized full rooftop" basis functions by merely combining the two "generalized half rooftop" basis functions [Fig. 1(d)], we assumed that the presence of the metallization at the other side of the artificial port does not alter the "generalized half rooftops." In order to take the coupling between the metallizations of two subcircuits across an artificial port into account, we can construct these "generalized full rooftop" functions directly. Starting from the subdivided circuit [Figs. 1(b) and 2(a)], we combine the metallizations of two continuous subcircuits across an artificial port [Fig. 2(b)] and use this combination in the lower level MoM by exciting their common (lower level) port. The resulting "generalized full rooftop" profiles [Fig. 2(c)] will be more accurate than those from Fig. 1(d) because the (field) coupling across the artificial port is taken into account. These "generalized rooftop" basis functions are again used as the basis functions for the upper level MoM, just like in the previous subsection.

In [12], this pairing technique was applied to the simulation of (wire) antennas, facilitating the implementation of the excitation.

Artificial ports excited like this will be called fixed artificial ports (FAP's) in contrast with the split artificial ports (SAP's) where two simulations and two "generalized half rooftops" are used before uniting them into a single "generalized full rooftop."

III. Iterative Refinement

A. Introduction

During the simulation of the lower level in the MMM, the presence of metallizations other than the subcircuit considered is neglected. This can be a cause of inaccuracy and errors in

the final result. In the case of FAP's the error will be smaller, but the metallization of the subcircuits not connected to the considered artificial port will be neglected and this omission will introduce errors. In order to reduce the errors, an iterative technique converging to the exact solution can be put forward.

As a first possibility, the final current profiles I_{ie} from (3) can be iteratively corrected in order to take each coupling into account. The profiles found by the upper level MoM [Fig. 1(e)] can be used as the starting point for a linear block iterative method such as block Gauss–Seidel (BGS), back–forth BGSf, and block Jacobi [20]–[22]. These methods turned out to be insufficiently stable to converge even for simple transmission lines. Therefore, this approach was aborted.

B. Basis Function Iterations

As we have a two-level MMM, the iterative correction can be applied to both levels. However, there are several reasons for applying an iterative technique to the lower level basis functions.

1) The upper level currents are not accurate (enough) due to the omission of the other metallizations. Iteratively including these neglected metallizations could overcome the problem.
2) As the upper level MoM simulation will be applied to the results of the iteration, the reduction of the error on the basis functions due to the iteration will still be further reduced by the variational nature of the MoM [11], [19]. Thus, the iterative correction of the lower level results will be more effective and lead to better convergence.
3) The overall current profiles are a linear combination of basis functions. Thus, the dimensionality of the lower level is higher than that of the upper level and has more degrees of freedom than the upper level. Hence, this iteration is likely to be more stable.
4) Perhaps the most important reason is based on diakoptics [11], [12], [14], making it possible to prove that if the basis functions converge to the so-called diakoptic basis functions, the overall solution based on these basis functions will match the full solution—i.e., the solution from one direct MoM—exactly (apart from numerical inaccuracies). Indeed, in general, diakoptics state the following [14]: given a set of basis functions, some of these are selected as special ones and a new set of basis functions is constructed by exciting each of the selected functions separately; in that case, the range of solutions of the old set of basis functions and the range of solutions of the new set are the same. The new basis functions are called the diakoptic basis functions.

We apply diakoptics to our two-level MMM in the following way. Our original set of basis functions is formed by the lowest level rooftop functions over the sides i. We select the rooftops over the portsides of the lower level ports (both exterior ports and artificial ports) as special functions, and we iteratively construct the profiles BF_k resulting from exciting each of these lower level ports separately. If we use these (diakoptic) profiles as basis functions for the upper level MoM, the resulting overall current profiles will exactly match the profiles found by one direct MoM [14].

In the proposed iterative approach, the subsectional (i.e., only defined on the subcircuits connected to the considered lower level port) upper level "general (full) rooftop" basis functions are extended into full-domain (i.e., defined over the complete circuit) diakoptic basis functions. We developed two iterative techniques which turned out to be very suitable to construct these diakoptic basis functions. They are described in the following subsections.

C. Modified Diakoptics (MD)

The first method is based on the MD [12] and has a physical interpretation. We will illustrate this interpretation using the "generalized rooftop" basis function BF_4 from the transmission-line example of the previous section (Figs. 1 and 2). During the lower level MoM simulation, no metallization other than that of the subcircuits connected to the considered artificial port (subcircuits (3) and (4) in the example) is taken into account, thus there is no current on the other metallizations [Fig. 3(a)]. The currents on each of these subcircuits will excite currents on all the other subcircuits by (first-order) field coupling (Fig. 3(b) shows how subcircuit (3) acts as a sending antenna and subcircuits (1) and (2) as receiving antennas). During the first iteration, these first-order coupling currents are calculated. These currents will, in turn, excite (second-order) coupling currents on all the other subcircuits (Fig. 3(c) shows how, with subcircuit (2) as sending antenna, subcircuits (1), (3), and (4) act as receiving antennas). These are calculated in the second iteration. These currents will again excite currents on all the other subcircuits, and so forth. The actual current is the sum of the lower level MoM current—say, the zeroth-order coupling current, Fig. 3(a)—and the currents from the different iterations—the nth order coupling currents—and can be seen in Fig. 3(d). Remark that there is no current on the portsides of all lower level ports LP_k, except at the excited one (LP_4 in Fig. 3).

The actual current profile [Fig. 3(d)] should be a good approximation of the diakoptic basis function belonging to the considered port. Note that the basis functions have become full-domain basis functions [Fig. 3(d)], whereas the original "generalized rooftop" basis functions were subsectional [Figs. 1(d), 2(c), or 3(a)].

The calculation of the first-order coupling currents differs somewhat between FAP's and SAP's. For FAP's, the coupling between the subcircuits across the considered artificial port [subcircuits (3) and (4) in Fig. 3(a)] is already taken into account during the lower level MoM simulation [Fig. 2(b) and (c)] and, therefore, there will be no first-order coupling current on these subcircuits. For SAP's, this coupling is not yet taken into account during the lower level MoM simulation [Figs. 1(b) and 2(c)] and a first-order coupling current will be excited on these subcircuits [if lower level port LP_4 (artificial port AP_3) were a SAP, there should be an extra current on subcircuit (4) in Fig. 3(b)].

For the first-order coupling of each basis function, only the two subcircuits across the excited artificial port have to be con-

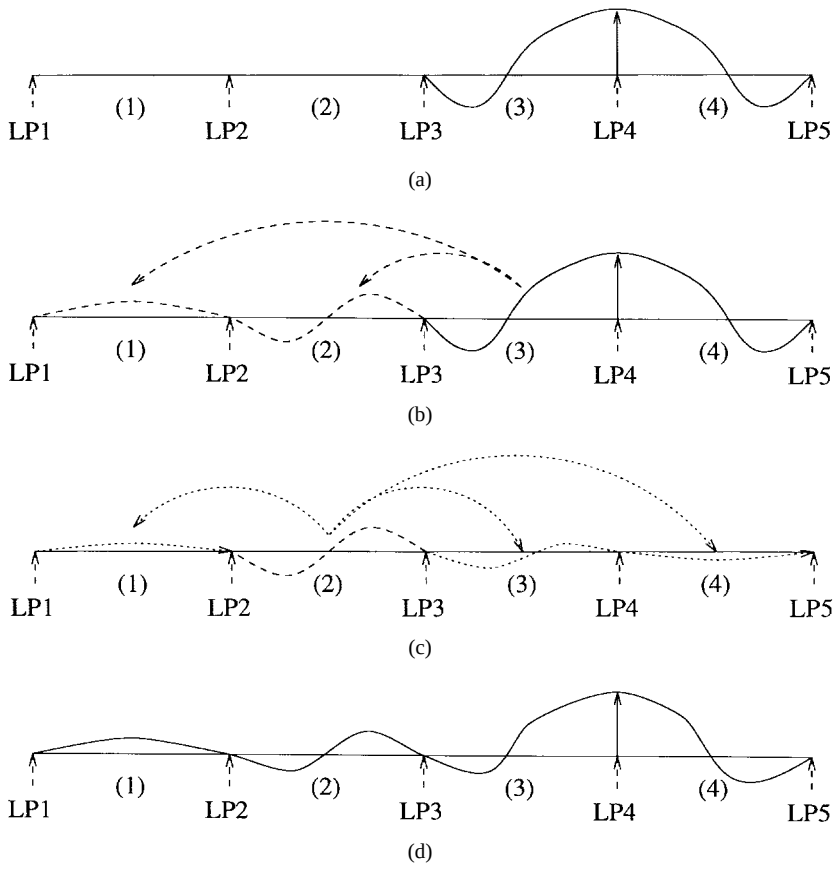

Fig. 3. Modified diakoptics.

sidered as sending antennas (only they carry current), whereas from the second-order coupling onwards, all subcircuits have to be considered as sending antennas.

In order to simplify the notation, we will combine the sides in the complete circuit into blocks of sides: all the sides belonging to the same subcircuit (excluding the portsides of the connected lower level ports) are combined into one block for each subcircuit; all the portsides belonging to the same lower level port are also combined into one block for each lower level port. Assuming S subcircuits (s) and L lower level ports LP_l, there are S subcircuit blocks and L lower level port blocks and L basis function BF_k (in Fig. 3, $S = 4$ and $L = 5$). These blocks of circuit sides and portsides are then ordered in ascending order of subcircuit number $(1, 2, \cdots, S)$, respectively, lower level port numbers $(1, 2, \cdots, L)$, the subcircuit blocks preceding the port blocks.

The matrix $[I_{ik}^{\mathrm{bf}}]$ describing the current density at side i of basis function BF_k is divided into block vectors I_{sk}^{S} and I_{lk}^{P} containing the current densities of the basis function BF_k for the sides belonging to the subcircuit (s), respectively, the sides belonging to the lower level port LP_l. The matrix $[Z_{ij}]$ describing the coupling between the (lowest level) rooftops over side i and side j is likewise divided into block matrices Z_{st}^{S}, coupling between the sides of subcircuit (s) and those of subcircuit (t), Z_{sl}^{SP}, coupling between the sides of subcircuit (s) and those of lower level port LP_l, and Z_{lm}^{P}, coupling between the sides of lower level port LP_l and those of lower level port LP_m.

When applying a diakoptic current excitation for basis function BF_k, only the lower level port LP_k is excited; hence,

$$I_{lk}^{\mathrm{P}} = [0], \qquad \text{for } l \neq k. \tag{4}$$

Taking this into account, the (block) matrix equation for the diakoptic basis functions becomes

$$\forall s = 1, \cdots, S, \forall k = 1, \cdots, L: \quad \sum_{t=1}^{S} Z_{st}^{\mathrm{S}} I_{tk}^{\mathrm{S}} = -\sum_{l=1}^{L} Z_{sl}^{\mathrm{SP}} I_{lk}^{\mathrm{P}} = -Z_{sk}^{\mathrm{SP}} I_{kk}^{\mathrm{P}}. \tag{5}$$

During the nth iteration, we use the standard iterative construction

$$I_{sk}^{\mathrm{S}}(n) = I_{sk}^{\mathrm{S}}(n-1) + \Delta I_{sk}^{\mathrm{S}}(n) \tag{6}$$

with $\Delta I^{\mathrm{S}}(n)$ the nth-order coupling current excited by the current $\Delta I^{\mathrm{S}}(n-1)$, initializing $I^{\mathrm{S}}(0)$ $[= \Delta I^{\mathrm{S}}(0)]$ with the "generalized rooftop" currents from the lower level MoM. Substituting (6) into the block matrix equation (5) and omitting the coupling between the highest order coupling currents, the block iteration formulas for basis function BF_k are

$$\Delta I_{sk}^{\mathrm{S}}(1) = \begin{cases} 0, & \text{if } s = t_{1,2} \\ -(Z_{ss}^{\mathrm{S}})^{-1}[Z_{sk}^{\mathrm{SP}} I_{kk}^{\mathrm{P}} + Z_{st_1}^{\mathrm{S}} I_{t_1 k}^{\mathrm{S}} & \\ \qquad + Z_{st_2}^{\mathrm{S}} I_{t_2 k}^{\mathrm{S}}], & \text{if } s \neq t_{1,2} \end{cases} \tag{7}$$

$$\Delta I^{\mathrm{S}}_{sk}(n) = -(Z^{\mathrm{S}}_{ss})^{-1}\left[\sum_{\substack{t=1\\ t\neq k}}^{S} Z^{\mathrm{S}}_{st}\Delta I^{\mathrm{S}}_{tk}(n-1)\right] \tag{8}$$

with $t_{1,2}$ the subcircuits connected to lower level port LP_k (in Fig. 3 $t_{1,2}$ are subcircuits (3) and (4) for LP_4).

Note that during each iteration, only the off-diagonal Z-matrix blocks (Z^{S}_{st} and Z^{SP}_{sk}) and the inverse of the diagonal Z-matrix blocks [$(Z^{\mathrm{S}}_{ss})^{-1}$) are needed (as was the purpose of our technique] together with the results of the previous iteration ($\Delta I^{\mathrm{S}}_{tk}(n-1)$). After each iteration the (previous) overall currents $I^{\mathrm{S}}_{sk}(n-1)$ are updated with the new additional currents $\Delta I^{\mathrm{S}}_{sk}(n)$ using (6) and the stop criterion (see below) is checked. If it is satisfied, indicating the approximation is "good enough," the iterative process is stopped or else a new iteration is started.

D. BGS

In the MD technique, the results of each step in the iteration (7), (8) are updated into the overall currents, but after the complete iteration (6), just as in the standard block Jacobi linear iterative technique [21], [22]. Jacobi's technique can be accelerated by updating the results of each step immediately [21], [22], resulting in Gauss–Seidel's method [20], or BGS for block matrices.

Introducing the recursion formula (6) into the diakoptic matrix equation (5) and using the most up-to-date currents available, the nth-order coupling currents can be found as

$$\Delta I^{\mathrm{S}}_{sk}(n) = -(Z^{\mathrm{S}}_{ss})^{-1}\left[Z^{\mathrm{SP}}_{sk}I^{\mathrm{P}}_{kk} + \sum_{t=1}^{s-1} Z^{\mathrm{S}}_{st}I^{\mathrm{S}}_{tk}(n) + \sum_{t=s}^{S} Z^{\mathrm{S}}_{st}I^{\mathrm{S}}_{tk}(n-1)\right]. \tag{9}$$

This equation can be further reduced by calculating the updated current $I^{\mathrm{S}}_{sk}(n)$ directly. When substituting (9) into the recursion formula (6), the BGS iteration formula becomes

$$I^{\mathrm{S}}_{sk}(n) = -(Z^{\mathrm{S}}_{ss})^{-1}\left[Z^{\mathrm{SP}}_{sk}I^{\mathrm{P}}_{kk} + \sum_{t=1}^{s-1} Z^{\mathrm{S}}_{st}I^{\mathrm{S}}_{tk}(n) + \sum_{t=s+1}^{S} Z^{\mathrm{S}}_{st}I^{\mathrm{S}}_{tk}(n-1)\right]. \tag{10}$$

The iteration formulas for MD and BGS—respectively, (8) and (10)—are completely analogous, apart from the influence of the excited lower level port for BGS [the first term between the brackets in (10)]. This seems to make BGS less computationally efficient as MD. However, the multiplication $Z^{\mathrm{SP}}_{sk}I^{\mathrm{P}}_{kk}$ is iteration independent and can, therefore, be done beforehand and stored in a matrix. From a computational viewpoint, this reduces this multiplication to an assignment. This assignment/multiplication is equivalent with the sum in the iterative construction (6) during the updating phase for the MD method and can also be seen in the first MD iteration (7). Thus, the number of operations per iteration are the same for BGS and MD.

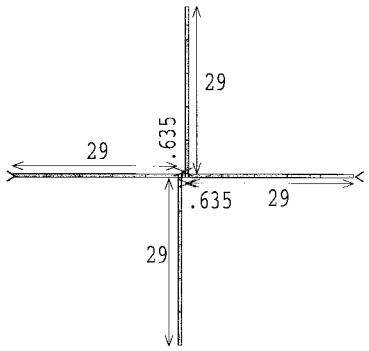

Fig. 4. Layout of a double-stub filter with five subcircuits.

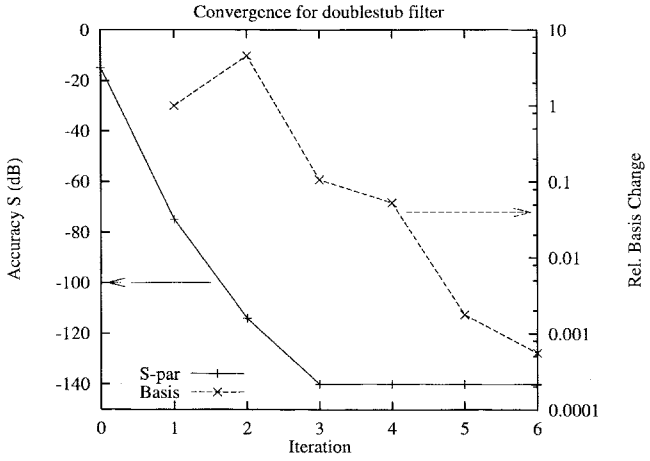

Fig. 5. Convergence of the double-stub filter with five subcircuits.

E. Stop Criterion

The iterative process is stopped when the number of iterations exceeds a given maximum (e.g., 20)—to interrupt a diverging process—or if the iterative correction becomes smaller than a tolerance (e.g., 0.1%)—the solution has converged. For the calculation of that correction, a continuous weighted relative-absolute norm formula was taken, comparing the additional basis function current for each side and excitation with the current from the previous iteration

$$\mathrm{Corr}(n) = \max_{\substack{\text{side } i\\ \text{BF } k}}\left\{\frac{|\Delta I^{\mathrm{bf}}_{ik}(n)|}{\max\left\{|I^{\mathrm{bf}}_{ik}(n-1)|,\ 10^{-4}\cdot\max_{\substack{\text{side } j\\ \text{BF } l}}|I^{\mathrm{bf}}_{jl}(n-1)|\right\}}\right\}. \tag{11}$$

This correction factor is assumed to be a measure for the accuracy of the iterative solution.

F. Acceleration of the Upper Level

When using diakoptics-based iterative refinement, the basis functions span the complete circuit, as can be seen in Fig. 3(d). Therefore, $\mathcal{O}(n^2)$ operations are needed to calculate (2), n being the total number of unknown currents. The following acceleration reduces the number of operations to $\mathcal{O}(n)$. The

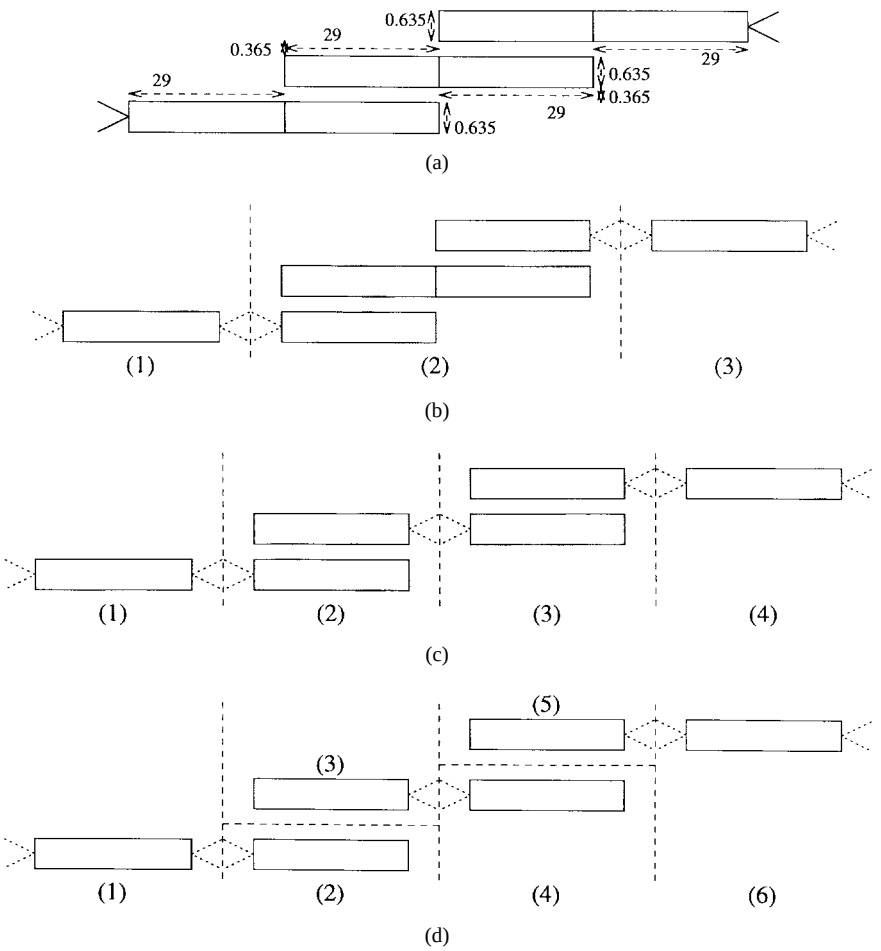

Fig. 6. Layout and several division schemes for a bandpass filter.

diakoptic basis functions are only excited by a (current) source at the corresponding lower level port. Therefore, there is only a localized incident electrical field at the lower level ports; the overall tangential electrical field vanishes at all other metallization (5). Hence, the basis function current distributions satisfy the matrix equation

$$\forall l \in LP: \forall i \notin LP(l): \sum_{j=1}^{n} Z_{ij} I_{jl}^{\mathrm{bf}} = E_{il}^{\mathrm{sc}} = -E_{il}^{\mathrm{in}} = 0 \tag{12}$$

with E^{sc} and E^{in} the scattered and the incident tangential electrical field, respectively. Thus, (2) reduces to

$$Z_{kl}^{\mathrm{up}} = \sum_{i \in \mathrm{LP}(k)} I_{ik}^{\mathrm{bf}} \sum_{j=1}^{n} Z_{ij} I_{jl}^{\mathrm{bf}} \tag{13}$$

needing only $\mathcal{O}(n)$ operations.

IV. Numerical Examples

A. Double-Stub Filter

This first simple example is intended to show that our iterative technique converges to the correct solution. A double-stub filter on 25-mil alumina ($\epsilon_r = 9.9$), the layout of which is given in Fig. 4 (dimensions in millimeters), was divided into five substructures (four quarter-wavelength sections—29 mm $\times$ 0.635 mm—and the central section—3 $\times$ 0.635 mm $\times$ 0.635 mm)—and simulated at 1 GHz. Reference data were obtained by simulating the filter as a whole. The convergence of the S-parameters (S_{11}, S_{12}, and S_{22}) and the basis functions can be seen in Fig. 5. Only six decimals of the S-parameters were taken into account, therefore, the maximum accuracy is -140 dB. The convergence of the S-parameters is more than exponential. The total number of unknowns was 24 for this example and only MD was used.

B. Bandpass Filter

The following example is a microstrip bandpass filter on 25-mil alumina ($\epsilon_r = 9.9$) consisting of three pairs of quarter-wavelength lines (QWL) with dimensions 29 mm $\times$ 0.635 mm, laterally separated by a 0.365-mm gap [see Fig. 6(a)]. The filter was simulated using MD and five different division schemes: as a whole [Fig. 6(a)] for reference data; divided in three [Fig. 6(b)], in four [Fig. 6(c)], and in six [Fig. 6(d)] using SAP's; and divided in six [Fig. 6(d)] using FAP's. The frequency was swept from 0.9 GHz up to 1.1 GHz using 21 equidistant samples. The curves for 4SAP and 6SAP are visually so close to each other that for visibility only the curves for 6SAP are plotted.

Fig. 7(a) shows the reflection ($|S_{11}|$) curves for the direct solutions (no iteration done), Fig. 7(b) those after one iteration. The direct solution of 6FAP is the best as it simulates the

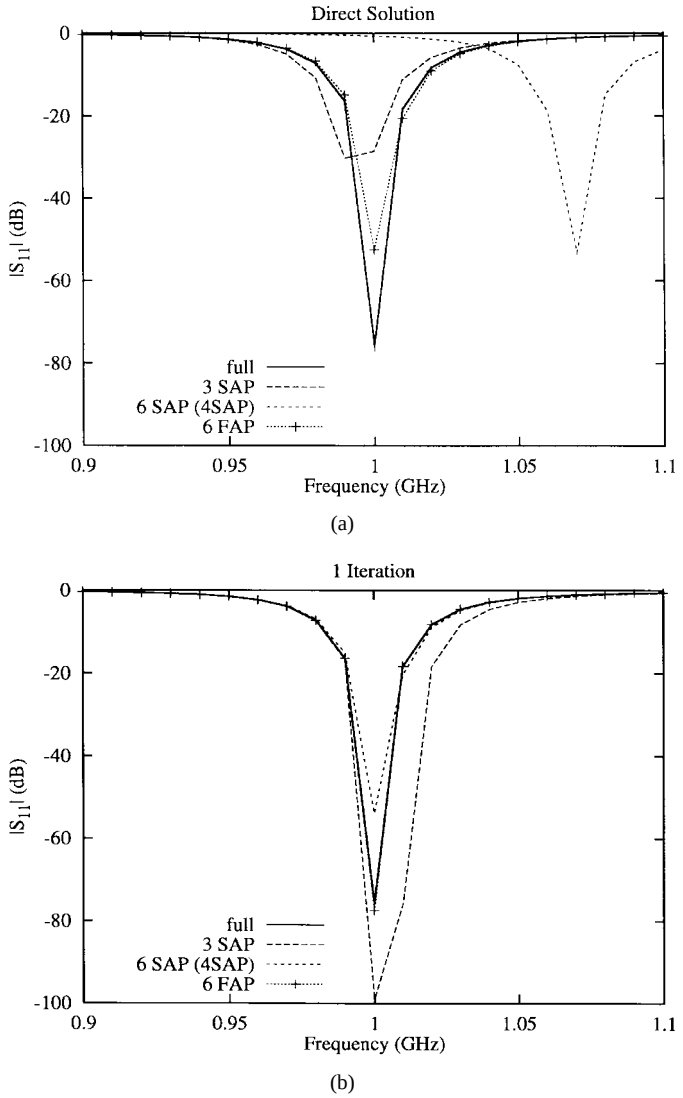

Fig. 7. Reflection coefficient (S_{11}) of the bandpass filter after direct solution and after one iteration.

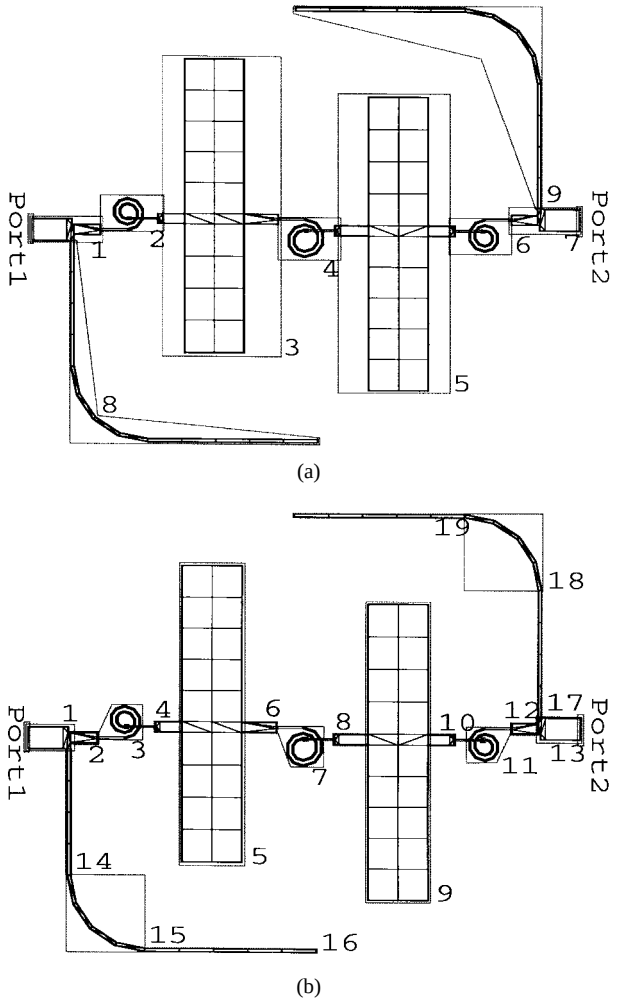

Fig. 8. Low-pass filter with (a) nine and (b) 19 divisions.

three pairs of QWL's as one part; 3SAP is less accurate as it simulates only the central pair as one; 6SAP (and 4SAP) mispredict the resonant frequency. After one iteration, 6FAP is very close to the correct result, followed by 6SAP (and 4SAP), which now have found the correct resonant frequency, but still overestimate the reflection; 3SAP, on the contrary, is the least accurate as it underestimates the reflection due to the small number of subcircuits.

After two or more iterations, the curves are visually the same. The largest difference with the reference curve is then smaller than -60 dB. The number of iterations needed for a correction smaller than 0.1% was independent from the frequency and ranged from six iterations for three divisions to eight iterations for six divisions. This shows that our technique is stable both for different division schemes and for different frequencies.

C. Low-Pass Filter

1) Description and Layout: As a third more elaborate example, we apply our technique to the simulation of a low-pass filter, the layout of which is given in Fig. 8. It consists of an input section—1 in Fig. 8(b)—with a folded matching stub—14–16 in Fig. 8(b), a step in width—2 in Fig. 8(b), a central section with three spiral inductors and two patch capacitors—3–4, 7–8, and 10–11, respectively, 5 and 9 in Fig. 8(b), a step in width—12 in Fig. 8(b)—and finally an output section—13 in Fig. 8(b)—with a folded matching stub—17–19 in Fig. 8(b). The overall circuit is quasi-symmetric (except for the inductors) and measures approximately 14 mm $\times$ 12 mm.

This circuit was gridded using rectangles and triangles, once with one transversal cell (except for the capacitor patches) and once using an edge mesh [23] (three transversal cells), yielding, respectively, 349 and 825 unknown variables. This circuit was divided into nine [Fig. 8(a)], 12, and 19 [Fig. 8(b)] parts. All circuits were simulated using SAP's and the nine divisions circuit also using FAP's. All those simulations were performed for both MD and BGS iterations for both normal and accelerated upper level, and for both the normal case and the edge mesh case. The normal case was simulated in the frequency interval 1–4 GHz using 16 equidistant frequency points; the edge mesh case was only simulated at 1 GHz.

The simulations were named according to the scheme "$xx[FS][b][a]$" in which "xx" indicates the number of divisions, "F," and "S," respectively, FAP and SAP, "b"

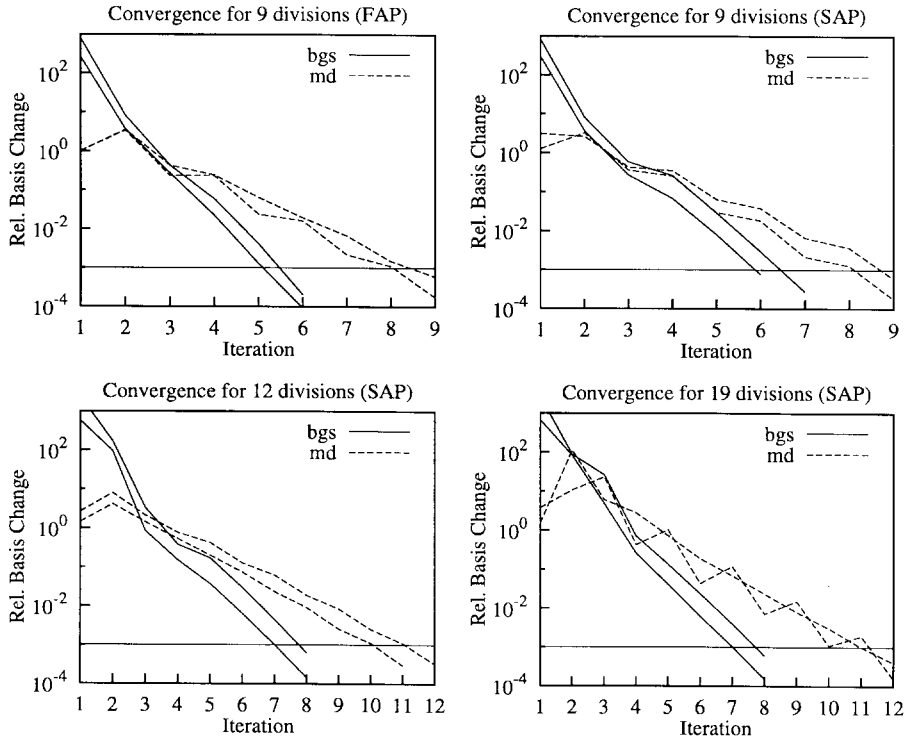

Fig. 9. Convergence of the basis functions of the low-pass filter.

BGS (MD in the absence of "b") and "a" accelerated upper level (normal upper level in the absence of "a"). The iterative process was stopped for corrections lower than 0.1% or after 20 iterations. Thus, we strive to obtain an accuracy of (more than) -80 dB on the S-parameters (see below).

The reference situation was obtained by simulating the complete circuit as a whole ("*full*") for the normal case as well as for the edge mesh case.

2) Convergence and Accuracy: Fig. 9 shows how the relative basis change or correction (11) diminishes with increasing number of iterations for the four division strategies with upper level iteration and the smaller case ($n = 349$). The curves, at 1 and 4 GHz, for BGS decrease monotonous and faster than the not so uniformly descending curves for MD. This proves that the BGS technique indeed converges faster than the MD technique as was expected (see Section III). The same conclusions hold for the edge mesh case ($n = 825$). Note that the accelerated upper level has no influence on the basis function iterations and, therefore, gives the same curves.

Fig. 10 shows the accuracy of the S-parameters during the iterative process. The curves (at 1–4 GHz) are grouped per iteration strategy (BGS or MD) and per upper level simulation technique (accelerated or not) and are merely meant for qualitative purposes. For each simulation, the arrows indicate the total range in numbers of iterations covered by the four frequencies, and this at the accuracy of -80 dB. The accuracy was calculated as the maximum absolute difference between the "*full*" simulation and the considered simulation for both real and imaginary part of all S-parameters. For the four division strategies, BGS converges the fastest, followed by MD and BGS combined with accelerated upper level. MD combined with accelerated upper level does not reach an accuracy of -80 dB when the correction is lower than 0.1%. It is clear that the accelerated upper level performs worse than the normal upper level. The same conclusions also hold for the larger case (edge mesh with $n = 825$).

3) S-Parameters: The convergence of the S_{11}-parameter over the complete frequency range for BGS ($n = 349$) is illustrated in Fig. 11. After the direct solution, the curves for 9SAP, 12SAP, and 19SAP almost coincide, whereas the curve for 9FAP already shows a low-pass characteristic. The 9FAP simulation converges the fastest, followed by 9SAP and, finally, 12SAP and 19SAP. As FAP's already include the coupling across the artificial ports, their convergence is faster than for SAP's. The circuits with 12 and 19 divisions suffer somewhat from oversegmentation, thus reducing the convergence rate. After three iterations the difference between the curves is no longer visible.

4) Timing Results: Next we will compare the calculation times for the different simulations. All calculations were performed on an HP9000 workstation, with the program code written in C++ without any optimization. The total time in the tables is the time in seconds needed to obtain the overall current distributions for voltage excitations at the exterior ports, given the overall Z-matrix $[Z_{ij}]$ and the subcircuit division. The time needed for the calculation of the Z_{ij}'s is not taken into account. The upper part of Table I describes the timings for MD, the lower part those for BGS, Table II only those for BGS. The first three rows give the results for iteration until the correction is smaller than 0.001 (or 0.1%), i.e., the time for the complete iterative process, the number of iterations, and the obtained accuracy of the S-parameters. The next row shows the (mean) time needed for one single basis-function iteration. As our goal was to obtain

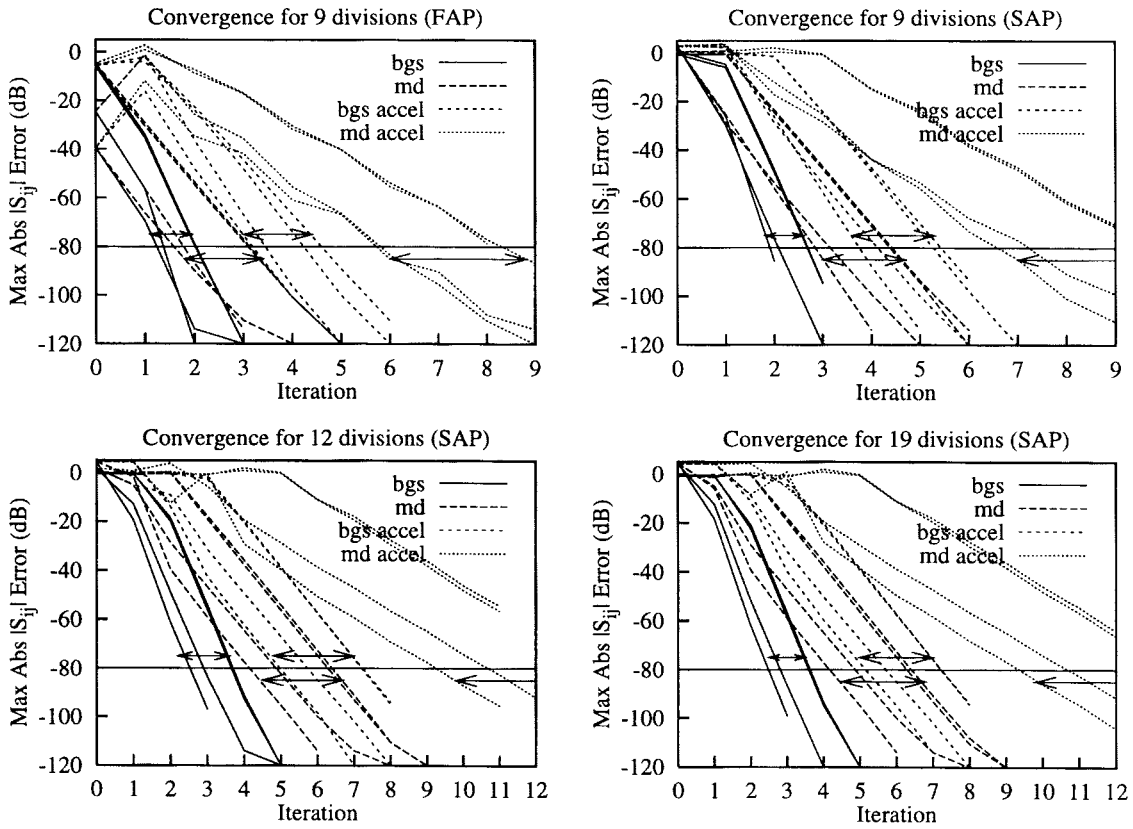

Fig. 10. Convergence of the S-parameters of the low-pass filter.

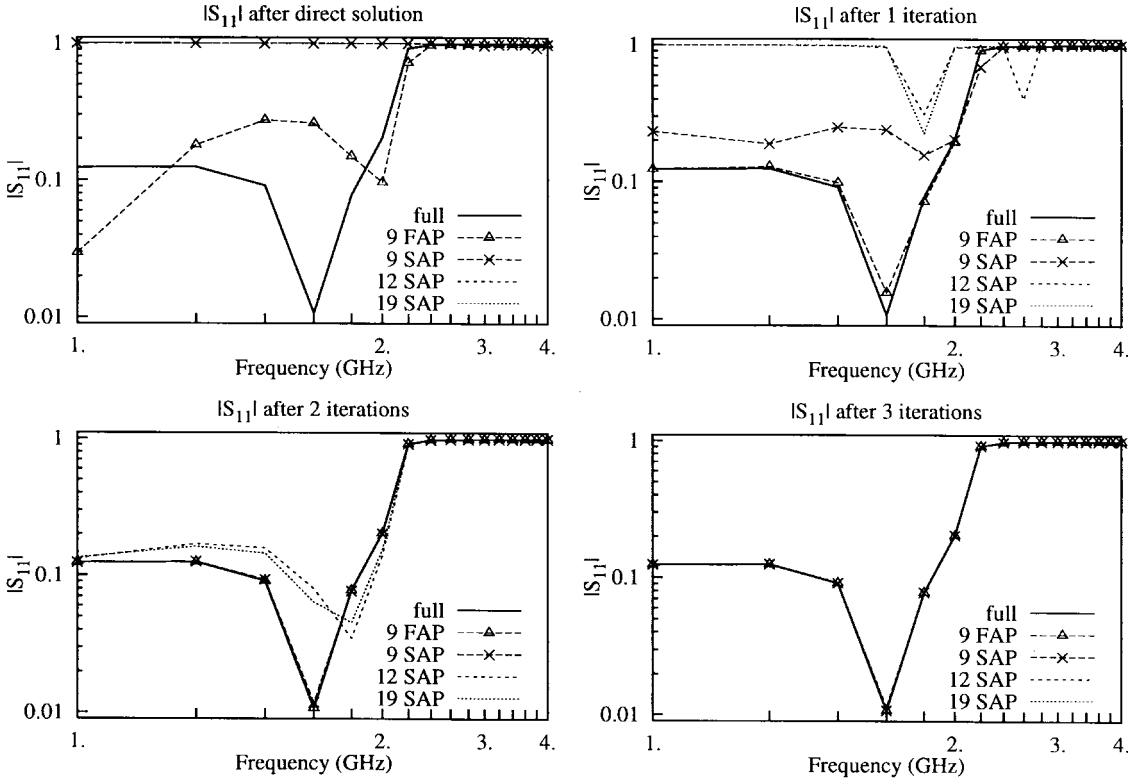

Fig. 11. Convergence of the reflection S-parameter (S_{11}) of the low-pass filter.

TABLE I
TIMING TABLE FOR THE LOW-PASS FILTER ($n = 349$) AT 1 GHz

Simulation (MD)	full	09F	09S	12S	19S	09Fa	09Sa	12Sa	19Sa
Total time (s)	23	33	32	43	74	30	28	38	64
Iterations		9	9	11	12	9	9	11	12
Accuracy (dB)		-140	-140	-140	-140	-87	-71	-56	-66
Time/iter (s)		3	3	3.5	5.5	3	3	3.5	5.5
Reduced Iters		4	5	7	7	9	9	11	12
Correction (%)		23→22	25→3	7→2	4→11	–	–	–	–
Reduced Time (s)	23	18	20	28	46	30	28	38	64
Simulation (BGS)	full	09Fb	09Sb	12Sb	19Sb	09Fba	09Sba	12Sba	19Sba
Total time (s)	23	26	24	33	54	22	21	29	44
Iterations		6	6	8	8	6	6	8	8
Accuracy (dB)		-140	-140	-140	-140	-110	-93	-94	-94
Time/iter (s)		3	3	3.5	5.5	3	3	3.5	5.5
Reduced Iters		3	3	4	4	5	6	8	8
Correction (%)		360→27	370→27	85→15	490→26	2→1	–	–	–
Reduced Time (s)	23	17	15	20	33	19	21	29	44

TABLE II
TIMING TABLE FOR THE LOW-PASS FILTER WITH EDGE MESH ($n = 825$) AT 1 GHz

Simulation (BGS)	full	09Fb	09Sb	12Sb	19Sb
Total time (s)	342	136	134	185	253
Iterations		6	7	8	8
Accuracy (dB)		-140	-140	-140	-140
Time/iter (s)		15	15	18	26
Reduced Iters		3	3	4	5
Correction (%)		800→17	800→33	130→29	280→20
Reduced Time (s)	342	92	90	110	176

an accuracy of −80 dB or better, we are interested in the smallest possible number of iterations to obtain that accuracy. This analysis was done after the complete iterative process. The last three rows of each part of the tables contain the results for an accuracy of −80 dB or better, i.e., the reduced number of iterations that suffice to obtain the −80-dB accuracy, the change of the correction in percentage in the basis functions during the second before last and the last of this reduced number of iterations and the reduced time accounting for the reduced number of iterations. The notation "25 → 3" in the "Correction" row of the MD simulation 09S, e.g., means that the fourth iteration (the second before last) had a basis correction of 25%, whereas the fifth (the last of the reduced iterations) had a correction of 3%. The last row is the most important one as it states whether the technique was more (or less) successful than a direct MoM simulation of the whole circuit (timing in the first column).

Note that the maximum possible accuracy is −140 dB as the S-parameter values are only compared up to 10^{-7} (6 decimals).

Table I shows that both MD and BGS have reached maximum accuracy after convergence, which cannot be said of the accelerated upper level technique. BGS converged in less iterations than MD. The number of iterations needed for an accuracy of −80 dB is again less for BGS than for MD, resulting in faster reduced times, for nine divisions, even faster than a full simulation (accelerated or not). MD without acceleration is also faster than a full simulation.

The results from Table I and the nonuniformly descending curves for MD in Fig. 9 show that for MD it is difficult to relate the basis function correction to the S-parameter accuracy. On the other hand, for BGS (not accelerated) a correction of approximately −3 dB in the basis functions results in an accuracy of −80 dB in the S-parameters; this relationship could be used as a better stop criterion. The times per iteration for MD and BGS (in combination with accelerated upper level or not) are the same for each simulation with the same number of divisions, as was expected from the theory.

The same conclusions hold for the other frequency points we used. The convergence for higher frequencies is even better due to the fact that the direct solution (before the iterative process starts) in the stopband (2–4 GHz) is already very close to the actual result (see Fig. 11), thus needing less iterations to yield the needed accuracy.

Summarizing for the smaller case, we can say that the use of BGS can reduce the solution time down to some 65% and MD down to some 78%. The accelerated upper level performs worse than the normal upper level. This is probably due to the fact that the condition (12) is not yet sufficiently fulfilled in order to allow for the acceleration (13).

Table II summarizes the most important timing results for the simulations using the edge mesh and BGS. The same conclusions can be drawn from Table II as from Table I. However, this time all simulation times are below the full simulation time and the difference between BGS and *full* and between BGS and MD (not shown here) has become larger. The time reduction now reaches up to a factor 3.8 for BGS in the best case and a factor of more than 2 for the other cases. A correction of −3 dB in the basis functions again corresponds to an accuracy of −80 dB in the S-parameters. The accelerated upper level (not shown here) again does not effectively accelerate the solution process due to reduced accuracy of (13). The acceleration technique should, therefore, not be considered any further.

V. CONCLUSIONS

In this paper, we introduced a combination of the MMM and diakoptics with an MD and a BGS iterative refinement. This reduces the solution time for the MoM matrix equation from an electromagnetic simulation, even for relatively small numbers

of variables. Different segmentations were taken and all proved successful, even oversegmentation. An accelerated upper level simulation was considered for both iterative techniques, but turned out ineffective or detrimental for further reducing the solution time. Several numerical examples were given and a new stop criterion—a correction of -3 dB in the basis function current densities—was suggested for an accuracy of -80 dB in the S-parameters. Further research is necessary to improve the accuracy if the (artificial) ports contain multiple sides and to assess the proposed stop criterion on other examples. Work is currently being done in these domains.

ACKNOWLEDGMENT

The authors wish to thank N. Faché for the fruitful discussions about the subjects mentioned in this paper.

REFERENCES

[1] R. F. Harrington, *Field Computations by Moment Methods.* New York: Macmillan, 1968.
[2] D. C. Chang and J. X. Zheng, "Electromagnetic modeling of passive circuit elements in MMIC," *IEEE Trans. Microwave Theory Tech.,* vol. 40, pp. 1741–1747, Sept. 1992.
[3] J. Sercu, N. Faché, F. Libbrecht, and P. Lagasse, "Mixed potential integral equation technique for hybrid microstrip-slotline multilayered circuits using a mixed rectangular–triangular mesh," *IEEE Trans. Microwave Theory Tech.,* vol. 43, pp. 1162–1172, May 1995.
[4] R. W. Jackson, "Full-wave, finite-element analysis of irregular microstrip discontinuities," *IEEE Trans. Microwave Theory Tech.,* vol. 37, pp. 81–89, Jan. 1989.
[5] T. Itoh, *Numerical Techniques for Microwave and Millimeter-Wave Passive Structures.* New York: Wiley, 1989.
[6] K. Umashankar and S. Nimmagadda, "Application of integral equation and method of moments for electrically very large scatterers using spatial decomposition technique," in *IEEE AP-S Int. Symp. Dig.,* vol. 1, Dallas, TX, May 8–10, 1990, pp. 76–79.
[7] K. R. Umashankar, S. Nimmagadda, and A. Taflove, "Numerical analysis of electromagnetic scattering by electrically large objects using spatial decomposition technique," *IEEE Trans. Antennas Propagat.,* vol. 40, pp. 867–877, Aug. 1992.
[8] E. Michielssen and A. Boag, "Multilevel evaluation of electromagnetic fields for the rapid solution of scattering problems," *Microwave Opt. Technol. Lett.,* vol. 7, no. 17, pp. 790–795, Dec. 5, 1994.
[9] ———, "A multilevel matrix decomposition algorithm for analyzing scattering from large structures," *IEEE Trans. Antennas Propagat.,* vol. 44, pp. 1086–1093, Aug. 1996.
[10] K. Kalbasi and K. R. Demarest, "A multilevel formulation of the method of moments," *IEEE Trans. Antennas Propagat.,* vol. 41, pp. 589–599, May 1993.
[11] G. Goubau, N. N. Puri, and F. Schwering, "Diakoptic theory for multielement antennas," *IEEE Trans. Antennas Propagat.,* vol. 30, pp. 15–26, Jan. 1982.
[12] F. Schwering, N. N. Puri, and C. M. Butler, "Modified diakoptic theory of antennas," *IEEE Trans. Antennas Propagat.,* vol. 34, pp. 1273–1281, Nov. 1986.
[13] E. Niver, H. H. Smith, and G. M. Whitman, "Frequency characterization of a thin linear antenna using diakoptic antenna theory," *IEEE Trans. Antennas Propagat.,* vol. 40, pp. 245–250, Mar. 1992.
[14] C. M. Butler, "Diakoptic theory and the moment method," in *IEEE AP-S Int. Symp. Dig.,* vol. 1, Dallas, TX, May 10, 1990, pp. 72–75.
[15] G. E. Howard and Y. L. Chow, "Diakoptic theory for the microstrip structures," in *IEEE AP-S Int. Symp. Dig.,* Dallas, TX, May 8–10, 1990, pp. 1079–1082.
[16] ———, "A high level complier for the electromagnetic modeling of complex circuits by geometrical partitioning," in *IEEE MTT-S Int. Symp. Dig.,* Boston, MA, June 10–14, 1991, pp. 1095–1098.
[17] C. F. Wang and D. G. Fang, "Multigrid method and diakoptic theory," in *IEEE AP-S Int. Symp. Dig.,* vol. 3, Newport Beach, CA, June 1995, pp. 1548–1551.
[18] A. John and R. H. Jansen, "From network theory toward field theory for (M)MIC chip level simulation," presented at the Proc. 24th European Microwave Conf. (EuMC), Cannes, France, Sept. 5–8, 1994.
[19] A. F. Peterson, D. R. Wilton, and R. E. Jorgenson, "Variational nature of Galerkin and non-Galerkin moment method solutions," *IEEE Trans. Antennas Propagat.,* vol. 44, pp. 500–503, Apr. 1996.
[20] R. Van Norton, "The solution of linear equations by the Gauss–Seidel method," in *Mathematical Methods for Digital Computers,* 10th ed., Ralson and Wilf, Eds. New York: Wiley, 1967, ch. 3, pp. 56–61.
[21] T. K. Sarkar, K. R. Siarkiewicz, and R. F. Stratton, "Survey of numerical methods for the solution of large systems of linear equations for electromagnetic field problems," *IEEE Trans. Antennas Propagat.,* vol. AP-29, pp. 847–856, Nov. 1981.
[22] O. Axelsson, *Iterative Solution Methods.* Cambridge, U.K.: Cambridge Univ. Press, 1994.
[23] N. Faché, "Advances in planar EM technology," *Microwave Eng. Europe,* Aug./Sept. 1995, pp. 55–60.

Steven Ooms (S'92) was born in Gent, Belgium, on May 8, 1970. He received the degree in electrotechnical engineering and the Ph.D. degree in electromagnetic simulations from the University of Gent, Belgium, in 1993 and 1997, respectively.

From October 1993 until June 1997, he was at the Department of Information Technology (INTEC), University of Gent, working as a Research Assistant for the Belgian National Funds for Scientific Research (NFWO). He is currently working for BARCO Chromatics, Belgium. His research focuses on the electromagnetic simulation of large circuits and the use of MMM.

Daniël De Zutter (M'92–SM'96) was born in Eeklo, Belgium, on November 8, 1953. He received the degree in electrical engineering, the Ph.D. degree, and the degree equivalent to the French Aggrégation or the German Habilitation from the University of Gent, Belgium, in 1976 and 1984, respectively.

From September 1976 to September 1984, he was a Research and Teaching Assistant in the Laboratory of Electromagnetism and Acoustics (now the Department of Information Technology), University of Gent, and is currently a Professor in the Department of Information Technology, and Research Director of the National Science Foundation of Belgium. He has authored, co-authored, and contributed to approximately 60 international journal papers and 70 papers in conference proceedings. Most of his earlier scientific work dealt with the electrodynamics of moving media, with emphasis on the Doppler effect and on Lorentz forces. His research now focuses on all aspects of circuit and electromagnetic modeling of high-speed and high-frequency interconnections, on electromagnetic compatibility (EMC) and electromagnetic interference (EMI) topics and on indoor propagation.

Dr. De Zutter was the recipient of the 1995 Microwave Prize Award.